RSC Applied Polymers

ROYAL SOCIETY OF CHEMISTRY

PAPER

View Article Online
View Journal | View Issue

Cite this: *RSC Appl. Polym.*, 2023, **1**, 64

Multifunctional MXene/PAA organohydrogel as a flexible strain sensor for wearable human–machine interaction†

Ning Ding,[a] Yan Bai,[a] Yuhui Feng,[a] Xiang Zou,[a] Yuzhe Chen,[a] Shuaihang Bi,[a] Shujuan Liu,[a] Weiwei Zhao *[a] and Qiang Zhao *[a,b]

Received 19th May 2023,
Accepted 7th July 2023

DOI: 10.1039/d3lp00052d

rsc.li/rscapplpolym

Flexible strain sensors play a critical role in wearable human–machine interaction (HMI), allowing for natural and intuitive communication between humans and machines. Conductive hydrogels are promising candidates for flexible sensor materials due to their flexibility, sensitivity, and biocompatibility. However, the conventional hydrogels tend to freeze at subzero temperatures or lose water at room temperature, resulting in decreased electrical conductivity and mechanical flexibility, and thus poor long-term stability. Herein, a multifunctional MXene/polyacrylic acid (PAA) organohydrogel with high toughness and self-healing, self-adhesive, antifreeze, and long-term moisturizing ability was prepared using a facile solvent replacement method. It has a high sensitivity (gauge factor ~10.96), wide detection range (0–1304%), and stable signal output for 500 cycles, making it an ideal flexible strain sensor for monitoring human joint movements, subtle expression changes, and pronunciation in real time. This work provides a new paradigm for wearable artificial intelligence and human–machine interactions in complex environments.

Introduction

In the past few years, the emergence of the "Metaverse" has stimulated the progress of various cutting-edge technologies.[1–3] Human–machine interaction (HMI) serves as a bridge for exchanging information and enabling interaction between the physical and virtual realms, allowing individuals to engage and maneuver in the virtual world through a variety of gestures and actions.[4–8] Flexible sensors are a critical component of HMI, enabling natural and intuitive communication between humans and machines.[9] To ensure effectiveness, these sensors must fulfill specific requirements, such as adaptability to human body curves and movements, tight adhesion to human tissues, and reliable real-time signal response.[10,11]

Hydrogel sensors are a promising candidate for monitoring human motion and providing natural and intuitive human–machine interactions in HMI applications due to their flexibility, sensitivity, biocompatibility, and durability.[4,12,13] However, practical application scenarios require sensors to have additional characteristics, such as great adhesion to different substrates,[14–16] self-healing for unavoidable wear or damage during use,[17–20] puncture resistance for contact with sharp and hard objects,[21,22] frost resistance for use in extremely cold environments,[23–25] and long-term moisture retention for working effectively under a variety of conditions.[26–28]

In view of these issues, organohydrogels, with organic compounds as the solvent, offer a promising solution.[29,30] The hydroxyl functional groups found in organic compounds are known to form numerous hydrogen bonds. These bonds serve a dual purpose by not only impeding the evaporation of water, but also inhibiting the formation of ice crystals, thus providing frost resistance.[31] However, most of the reported organohydrogels only address frost resistance and moisture retention, while neglecting the requirement for sensors with additional properties, such as self-healing and strong adhesion. There is an urgent need for novel sensors made of multifunctional organohydrogels that can satisfy the diverse demands in complex environments.

Herein, a multifunctional MXene/PAA organohydrogel is synthesized by a simple solvent displacement method. The organohydrogel exhibits excellent mechanical properties as well as impressive resistance to puncture. Its strong hydrogen bonding capability facilitates excellent adhesion to a variety of substrates and enables rapid self-healing in approximately 0.5

[a]*State Key Laboratory of Organic Electronics and Information Displays & Jiangsu Key Laboratory for Biosensors, Institute of Advanced Materials (IAM), Nanjing University of Posts & Telecommunications, 9 Wenyuan Road, Nanjing 210023, China. E-mail: iamwwzhao@njupt.edu.cn, iamqzhao@njupt.edu.cn*

[b]*College of Electronic and Optical Engineering & College of Flexible Electronics (Future Technology), Nanjing University of Posts & Telecommunications, 9 Wenyuan Road, Nanjing 210023, China*

† Electronic supplementary information (ESI) available. See DOI: https://doi.org/10.1039/d3lp00052d

s. Glycerol imparts the organohydrogel with exceptional anti-freeze and long-lasting moisturizing properties. These rich properties enable the MXene/PAA organohydrogel to meet various demands in complex challenging environments. Furthermore, MXene/PAA organohydrogel-based flexible strain sensors can monitor a variety of human joint movements with high reliability, and accurately capture physiological activities such as micro-expressions and throat pronunciation in real time. A set of wireless wearable flexible strain sensors have also been developed to monitor human movements, demonstrating the feasibility of the multifunctional MXene/PAA organohydrogel in practical applications. This work provides new insights into wearable flexible HMI electronics in complex environments.

Experimental section

Materials

Ti_3AlC_2 (200 mesh) was commercially purchased from Jilin 11 Technology Co., Ltd. Lithium fluoride (LiF) was purchased from Shanghai Aladdin Biochemical Technology Co., Ltd. Hydrochloric acid (HCl, 37%) and ammonium persulfate (APS) were obtained from Shanghai Sinopharm Group Co., Ltd. Acrylic acid (AA, 99%) was purchased from Energy Chemical Technology Co., Ltd. *N*,*N*′-Methylenebisacrylamide (MBAA) was purchased from Shanghai Macklin Biochemical Co., Ltd. Glycerol was commercially purchased from Xilong Science Co., Ltd. All chemicals were used without any further purification.

Characterization

The morphology and microstructure were characterized by scanning electron microscopy (SEM, Hitachi S-4800), transmission electron microscopy (TEM, Tecnai G2 F30 S-TWIN at 200 kV) and atomic force microscopy (AFM, Bruker ICON-Dimension). The elemental compositions were determined using an energy dispersive X-ray spectrometer (EDS, Horiba EX-250). Energy dispersive spectra and X-ray diffraction (XRD) patterns were obtained using an X-ray diffractometer (Bruker AXS D8 Advance) using Cu Kα radiation (λ = 1.5418 Å). Fourier transform infrared (FT-IR) spectra were obtained using an FT-IR spectrometer (PerkinElmer, PE-Spectrum Two). Attenuated total reflection Fourier-transform infrared (ATR-FTIR) spectra were obtained using an ATR-FTIR spectrometer (BRUKER, ALPHA II). The binding energies were measured by X-ray photoelectron spectroscopy (XPS, Kratos Axis Supra). Thermogravimetric analysis (TGA) was performed on an STA machine (NETZSCH STA2500 Regulus) at a rate of 10 °C min^{-1} to 650 °C under a nitrogen atmosphere. To facilitate SEM observation, the gel samples were subjected to freeze-drying treatment for three days using a freeze drying machine (BILON FD-1A-50). To facilitate FT-IR characterization, the gel samples were dried and ground to powder under an infrared heat lamp. For ATR-FTIR characterization, MXene/PAA organohydrogel samples were not further treated.

The stress–strain curves were obtained using a tensile testing machine (INSTRON 3365) with a stretching speed of 40 mm min^{-1} under ambient conditions. The tensile stress (σ) was calculated using the formula $\sigma = F/S$, where F and S denote the tensile load (N) and the initial cross-sectional area (m^2), respectively. The tensile strain (ε) was calculated using the formula $\varepsilon = (L - L_0)/L_0 \times 100\%$, where L_0 and L represent the initial length (mm) and the broken length (mm), respectively.[32]

The electrical conductivity of a rectangular hydrogel specimen (20 mm × 10 mm × 2 mm) was measured using electrochemical impedance spectroscopy (EIS) with an electrochemical workstation (CHI 660E). Conductivity (δ) was determined using the formula $\delta = L/(R \times S)$, where R (Ω), L (m) and S (m^2) represent the resistance, length and cross-sectional area, correspondingly.[33]

The storage modulus (G') and loss modulus (G'') of the hydrogels were measured using a rotational rheometer (DHR-1) with a frequency sweep of 10 rad s^{-1} over a temperature range from −30 to 25 °C. The MXene/PAA hydrogels and organohydrogels prepared *via* solvent replacement were placed in a closed environment to test the moisturizing properties. The ambient temperature was 20 °C and the humidity was 45%. Samples were collected every three hours to evaluate changes in quality.

Preparation of $Ti_3C_2T_X$ MXene nanosheets

MXene nanosheets were prepared by selectively etching the Al layer from Ti_3AlC_2 bulks using a modified LiF/HCl etching method, as described in a previous work.[34] Specifically, the etchant was prepared by adding 1 g of LiF to 20 mL of HCl (9 M) and then stirring for 20 min. Subsequently, 1 g of Ti_3AlC_2 powder was gradually added to the etchant and heated at 60 °C for 24 h. Afterward, the products were centrifuged at 3500 rpm several times with deionized water until the pH exceeded 6, and then dried under vacuum for 12 h. Next, multilayer MXene was dispersed in deionized water and sonicated under an argon flow for 1 h to obtain MXene nanosheets. Finally, after centrifugation at 3500 rpm for 1 h, an aqueous dispersion of MXene nanosheets was collected.

Synthesis of the MXene/PAA hydrogel and organohydrogel

First, 25 mg of APS and 2 mg of MBAA were dissolved in 3 mL of deionized water under magnetic stirring to prepare APS and MBAA mixed solution. Then, 0.25 mL of AA and 0.5 mL of the aqueous dispersion of MXene nanosheets were added to the as-prepared suspension, and the suspension was uniformly stirred in an ice-water bath.[35] Subsequently, the reaction was carried out at 60 °C for 4 h to form the MXene/PAA hydrogel. To prepare the MXene/PAA organohydrogel, the above hydrogel was soaked in glycerol solution for different times to promote solvent replacement.

Sensing test of the MXene/PAA organohydrogel

The electrical signal of the organohydrogel-based strain sensor was monitored with an amperometric *I–T* curve using an electrochemical workstation (CHI 660E) at a voltage of 1 V. To prepare the gel bioelectrode, the MXene/PAA organohydrogel was attached to a conductive wire. This gel bioelectrode was adhered to the skin for recording the electric current. The current signal was then transmitted wirelessly to the screen of

a mobile phone through a transmitting device, providing a non-invasive and convenient way to monitor human activity.

Results and discussion

Preparation and characterization of the MXene/PAA organohydrogel

The schematic illustration of the solvent replacement process and the crosslinking structure of the MXene/PAA organohydrogel are presented in Fig. 1a. First, an aqueous dispersion of MXene nanosheets was prepared by ultrasonic stripping of multilayered MXene bulks (Fig. S1†). Next, the AA monomer was mixed with the aqueous dispersion of MXene nanosheets, and then combined with a solution of APS and MBAA.[36] PAA was synthesized through the free radical polymerization of AA monomers, assisted by the chemical crosslinking agent MBAA and initiator APS.[37] Meanwhile, MXene nanosheets possess abundant surface-terminated functional groups (*i.e.*, –O, –F, and –OH) that facilitate hydrogen bonding interactions with carboxyl groups on PAA. Then, the MXene/PAA hydrogel was generated after heating at 60 °C for 4 h. Finally, the MXene/PAA organohydrogel was readily prepared by simple solvent replacement of the hydrogel (Fig. S3†). To be specific, the MXene/PAA hydrogel was immersed in the glycerol solvent. Driven by the difference in concentration, a part of the water was replaced by glycerol.[38] Organohydrogels with different water contents were obtained by controlling the displacement time (*i.e.*, 3 h, 6 h, 9 h, 12 h and 24 h).

To better understand the formation mechanism, the MXene/PAA organohydrogel was systematically characterized by SEM, EDS, XRD and XPS. The SEM image proved that the MXene/PAA organohydrogel possessed a three-dimensional (3D) porous structure (Fig. 1c). In comparison with the MXene/PAA hydrogel, the pore size of the MXene/PAA organohydrogel was slightly reduced, which corresponded to the macroscopic volume shrinkage of hydrogels before and after solvent displacement (Fig. 1b, S4 and S5†). EDS showed that elements such as C, F, O, and Ti were uniformly dispersed in the organohydrogel network. The XRD pattern of the MXene/PAA organohydrogel tended to be featureless compared to MXene nanosheets (Fig. S6†). This can be attributed to the complete encapsulation of MXene nanosheets during AA polymerization, resulting in their high dispersion in the organic hydrogel system.[36] The XPS spectrum of the MXene/PAA organohydrogel and MXene nanosheets also demonstrated that the

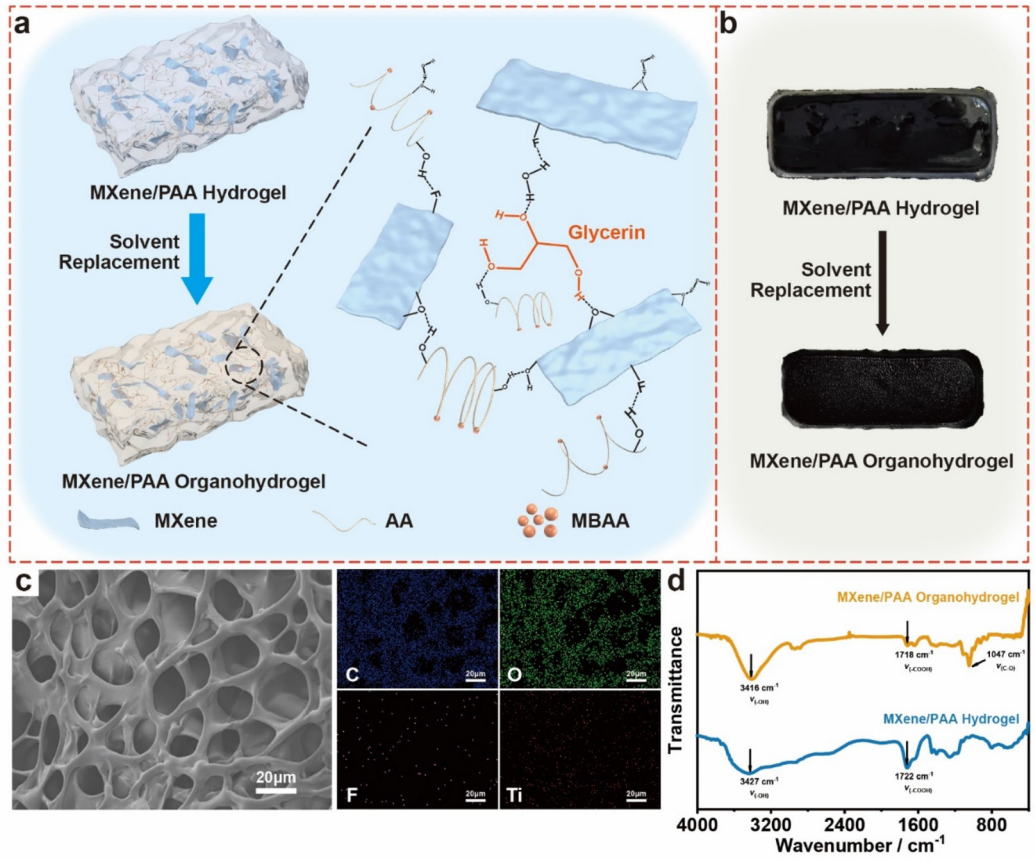

Fig. 1 (a) Schematic diagram of the solvent substitution process. (b) Photographs of the MXene/PAA hydrogel and the MXene/PAA organohydrogel. (c) SEM image and elemental mapping images of the MXene/PAA organohydrogel. (d) FT-IR spectra of the MXene/PAA hydrogel and the MXene/PAA organohydrogel.

MXene nanosheets were completely covered and wrapped by the PAA polymers (Fig. S7†).[36] The above results showed that the introduction of glycerol did not change the internal structure of the hydrogel, nor did it lead to the solidification and self-accumulation of MXene nanosheets. FT-IR spectroscopy provided more details for clarifying the introduction of glycerol (Fig. 1d). From the spectra of the MXene/PAA hydrogel, the peak at 1722 cm^{-1} was assigned to the –COOH group, and the peaks at 3427 cm^{-1} and 1640 cm^{-1} were assigned to the –OH group. In the MXene/PAA organohydrogel, these peaks shift to lower wavenumbers of 1718 cm^{-1} and 3416 cm^{-1}, due to the stronger hydrogen-bonding interactions between glycerol and polymer chains that further average the electron cloud density, thereby reducing the frequency of stretching vibrations.[39] In addition, a new characteristic peak at 1047 cm^{-1} appeared for the MXene/PAA organohydrogel, which was assigned to the C–O stretching vibration peak of glycerol (ν_{C-O}). These phenomena jointly reveal the increase of cross-linking density of the polymer network by the introduction of glycerol.[30,32]

Performance investigation of the MXene/PAA organohydrogel

The mechanical properties of the organohydrogel are crucial for practical applications. In this regard, the MXene/PAA organohydrogel exhibits excellent mechanical resilience, quickly returning to its initial state after bending, twisting, and stretching (Fig. 2a). To further explore the effect of glycerol on the mechanical properties, MXene/PAA organohydrogels with different replacement times (*i.e.*, 0 h, 3 h, 6 h, 9 h, 12 h and 24 h) were prepared. The effect of the replacement time on tensile properties is studied (Fig. 2b). The strain of organohydrogels increased from 1087% to 1346%, and the corresponding stress increased from 108.14 kPa to 207.18 kPa, with an increase in replacement time from 0 h to 9 h, demonstrating significantly increased ductility and toughness. However, as the replacement time further increased to 24 h, the strain decreased to 895%, and the stress decreased to 158.74 kPa. Hydrogels contain water molecules that exist in three forms: "free water", "intermediate water" and "bound water".[40] "Free water" can freely exchange with glycerol molecules and form hydrogen bonds with glycerol molecules because it is not bound to the gel network. The displacement process between "intermediate water" and "bound water" molecules and glycerol molecules occurs slowly as they are bound to the polymer network by hydrogen bonds. In the initial stage of the replacement process, "free water" is replaced by glycerol molecules, which increases the stress as well as the strain of hydrogels.

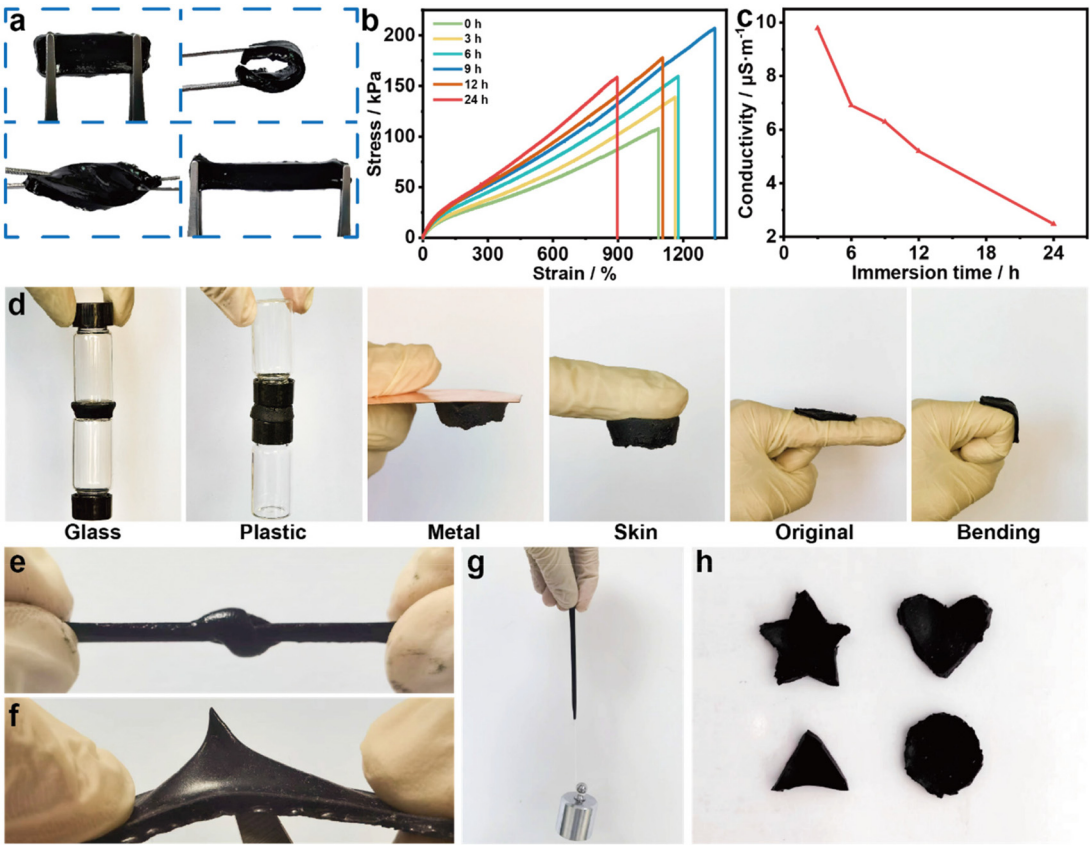

Fig. 2 Performance investigation of the composite organohydrogels. (a) Photographs of the flexible MXene/PAA organohydrogel in original, bent, twisted and stretched states. Stress–strain curves (b) and conductivity (c) of MXene/PAA organohydrogels with different replacement times. (d) Photographs of the MXene/PAA organohydrogel illustrating the adhesiveness to diverse surfaces. Photographs of the flexible MXene/PAA hydrogel on stretching after making a knot (e), bearing the sharp pressure of a scissor (f) and lifting 200 g weight (g) and shapeability (h).

With the further progress of the replacement, a large number of water molecules are further replaced with glycerol molecules, resulting in a slight decrease in the mechanical properties of the MXene/PAA organohydrogel.

In addition, the effect of different replacement times on the conductivity is investigated (Fig. 2c). With the increase of replacement time, the conductivity of the MXene/PAA organohydrogel decreased significantly. The main reason is that glycerol molecules replace some water molecules in the process of replacement, which inhibits the migration of ions.[31,38] The comparisons of the conductivity of pure MXene, hydrogels, and organogels have been provided in Table S1.† Considering the excellent mechanical and electrical properties, organohydrogels with a replacement time of 9 h were selected for subsequent characterization.

The majority of sensors need additional adhesives for attachment to either the human body or clothing, which can lead to skin irritation, poor flexibility, and low accuracy, ultimately hindering the sensor's application in wearable HMI electronics.[14,16] The MXene/PAA organohydrogel demonstrates exceptional adhesion characteristics to both hydrophilic and hydrophobic substrates, such as glass, plastic, metal, and skin (Fig. 2d). In the process of human activities, such as the bending of fingers, the organohydrogel can maintain close adhesion to the skin, showing excellent adhesion. Meanwhile, the gel can bear stretching and recover its original shape after being knotted, demonstrating great mechanical properties (Fig. 2e). Additionally, the gel with excellent puncture resistance could withstand pressure from sharp objects such as scissors without any surface cracks or scratches (Fig. 2f). The organohydrogel could also hold a load of 200 g without breaking, revealing its strong mechanical strength (Fig. 2g). Various shapes of organohydrogels, including stars, hearts, triangles, and circles, could be readily prepared, exhibiting impressive shapeability, which forms a solid foundation for flexible electronics (Fig. 2h).

The incorporation of reversible dynamic hydrogen bonds imparts the MXene/PAA organohydrogel with autonomous self-healing capability, which not only contributes to prolonging the material's lifespan but also enhances its long-term functionality and usability. In order to demonstrate the self-healing ability, the organohydrogel was connected to a red LED lamp *via* wires at a 3 V voltage. The integrity of the circuit was represented by the emission of red light from the LED lamp, as shown in Fig. 3a. When the organohydrogel was cut off, the LED light immediately went out. However, when the two separated pieces were brought into contact again, the LED lamp quickly lit up again. Real-time current changes during five consecutive repetitions of the cutting–contact process were recorded and shown in Fig. 3b. When the organohydrogel was cut off, the current dropped rapidly to 0 μA, but when the two separated gels were brought into contact again, the current quickly returned to the initial state. Remarkably, the conductive path was repaired in just 0.5 s, demonstrating the fast self-healing ability of the hydrogel. Moreover, the self-healing process was fully repeatable, and the organohydrogel maintained stable self-healing time and electrical conductivity during five consecutive disconnection processes. The self-healing ability of the MXene/PAA organohydrogel holds significant potential in wearable HMI electronics and enables the gel to withstand repeated mechanical stresses and damage, making it an ideal candidate for use in wearable electronic devices that require frequent bending and twisting.[41]

Compared to the MXene/PAA hydrogel, the MXene/PAA organohydrogel exhibits great flexibility and mechanical properties at low temperatures (Fig. 3c and d). To further evaluate the frost resistance, the rheological properties at different temperatures were studied. Fig. 3e and f show the rheological results of the MXene/PAA organohydrogel and the MXene/PAA hydrogel. Generally, in the temperature range from −30 to 25 °C, the storage modulus of hydrogels is always greater than the loss modulus, indicating the formation of a cross-linked network inside both the MXene/PAA hydrogel and the MXene/PAA organohydrogel.[42] The storage modulus and loss modulus of the MXene/PAA hydrogel decrease strongly at −12 °C, which is its freezing point. In contrast, the storage modulus and loss modulus of the organohydrogel maintain small values in the range from −30 °C to 25 °C. This is because the added glycerol molecules can break the hydrogen bonds in the ice crystals to effectively prevent the formation of ice crystals and further reduce the freezing point of the hydrogel.[32]

Conventional hydrogels face the challenge of maintaining their long-lasting moisturizing properties without drying.[27,43] In contrast, the MXene/PAA organohydrogel demonstrates excellent moisture retention abilities. Fig. 3g, S9 and S10† show the shape changes of the MXene/PAA hydrogel and the MXene/PAA organohydrogel after being placed for different times in a constant environment at a temperature of 20 °C and a humidity of 45%. In the test environment, due to the inevitable continuous evaporation of water from the MXene/PAA hydrogel, the volume of the hydrogel shrinks significantly after being placed for 24 h. In contrast, the organohydrogel with a replacement time of 9 h basically maintains the original shape for 81 h. To further characterize the moisturizing properties of the two hydrogels, the changes in the weight in the test environment are tested (Fig. 2h). The mass of the MXene/PAA hydrogel decreases rapidly; only 28% of the initial mass remains after 105 h, while the organohydrogel retains 96% of the initial mass. In addition, the ATR-FTIR spectra and TGA spectra also confirm the excellent water retention of the organohydrogel (Fig. S11 and S12†). The presence of glycerin, with its hydroxyl groups that effectively bind with water molecules, plays a crucial role in preventing water evaporation and sustaining the moisturizing effect of the gel.[31]

Sensing performance of the MXene/PAA organohydrogel

To assess the effectiveness of the MXene/PAA organohydrogel strain sensor, two pieces of copper foil are used to cover the gel for electrochemical measurement. The tensile sensitivity of the organohydrogel strain sensor is evaluated and the gauge factor (GF) is calculated by the slope of the relative resistance–strain curve (Fig. 4a). The GF is found to be 5.14 for the strain range of 0–270% and 10.96 for the strain range of 270–1304%.

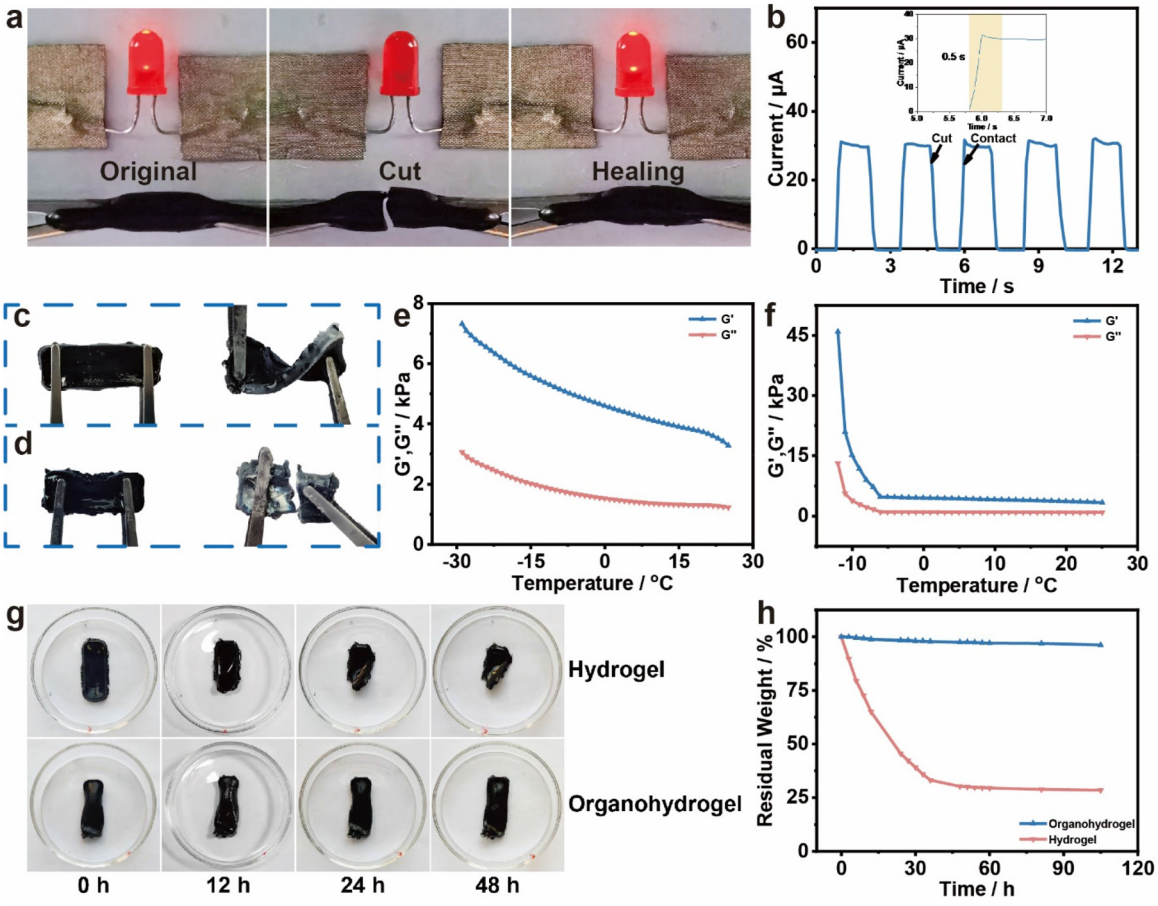

Fig. 3 (a) Photographs of LED brightness lit by the MXene/PAA organohydrogel in different states (*i.e.*, original, cut and healing). (b) Current change curves of the MXene/PAA organohydrogel before and after self-healing. Photographs of the flexible MXene/PAA organohydrogel in original and twisted states (c) and the MXene/PAA hydrogel in original and twisted states (d) at −20 °C. Storage modulus (*G*′) and loss modulus (*G*″) curves of the MXene/PAA organohydrogel in the temperature range from −30 °C to 25 °C (e) and the MXene/PAA hydrogel in the temperature range from −12 °C to 25 °C (f), photographs (g) and weight change curves (h) of the MXene/PAA hydrogel and the MXene/PAA organohydrogel after placing for different times at 20 °C and 45% humidity.

These changes in resistance are attributed to the alteration in the MXene based 3D conductive network, resulting in a rapid decrease in the conductive path microscopically and a sharp increase in the sensor resistance macroscopically, reaching a higher GF.[44] Compared to both the MXene/PAA hydrogel and other previously reported gels, the MXene/PAA organohydrogel displays superior sensitivity (Tables S2 and S3†). The sensing response of the organohydrogel under tensile deformation is shown to have stable repeatability in three consecutive cycles, proving its reliability as a strain sensor for monitoring various tensile strains (Fig. 4b). Additionally, the MXene/PAA organohydrogel strain sensor maintains sensitivity after undergoing 500 cycles of 30% strain, exhibiting high sensitivity, excellent stability, and repeatability (Fig. 4c).

The MXene/PAA organohydrogel exhibits significant potential as a non-irritating wearable strain sensor for real-time biomonitoring purposes. The excellent self-adhesive properties facilitate easy attachment to various body parts, including the fingers, wrist and elbow. It is worth emphasizing that previous studies have demonstrated the non-toxic characteristics and exceptional biocompatibility of the MXene/PAA hydrogel.[45] Furthermore, considering the widespread utilization of glycerol in the cosmetics and pharmaceutical industries, owing to its well-established non-toxic properties, the MXene/PAA organohydrogel can be confidently regarded as safe for skin application and holds promising prospects for wearable applications. The sensor accurately detects relative resistance changes at a certain bending angle, with a consistent and repeatable signal output (Fig. 4d–f). Apparently, the MXene/PAA organohydrogel based sensor can accurately detect human movement behavior of different joints. In addition, the wearable strain sensor can also accurately detect subtle human motion, including swallowing, smiling, frowning and even speaking (Fig. 4g–l). When used for voice monitoring, the sensor can accurately respond to each syllable in different words and exhibit high repeatability. It highlights the promising application potential of the MXene/PAA organohydrogel in the fields of motion detection and intelligent medicine. These promising results demonstrate the great potential of the MXene/PAA organohydrogel strain sensor for application in wearable HMI electronics.

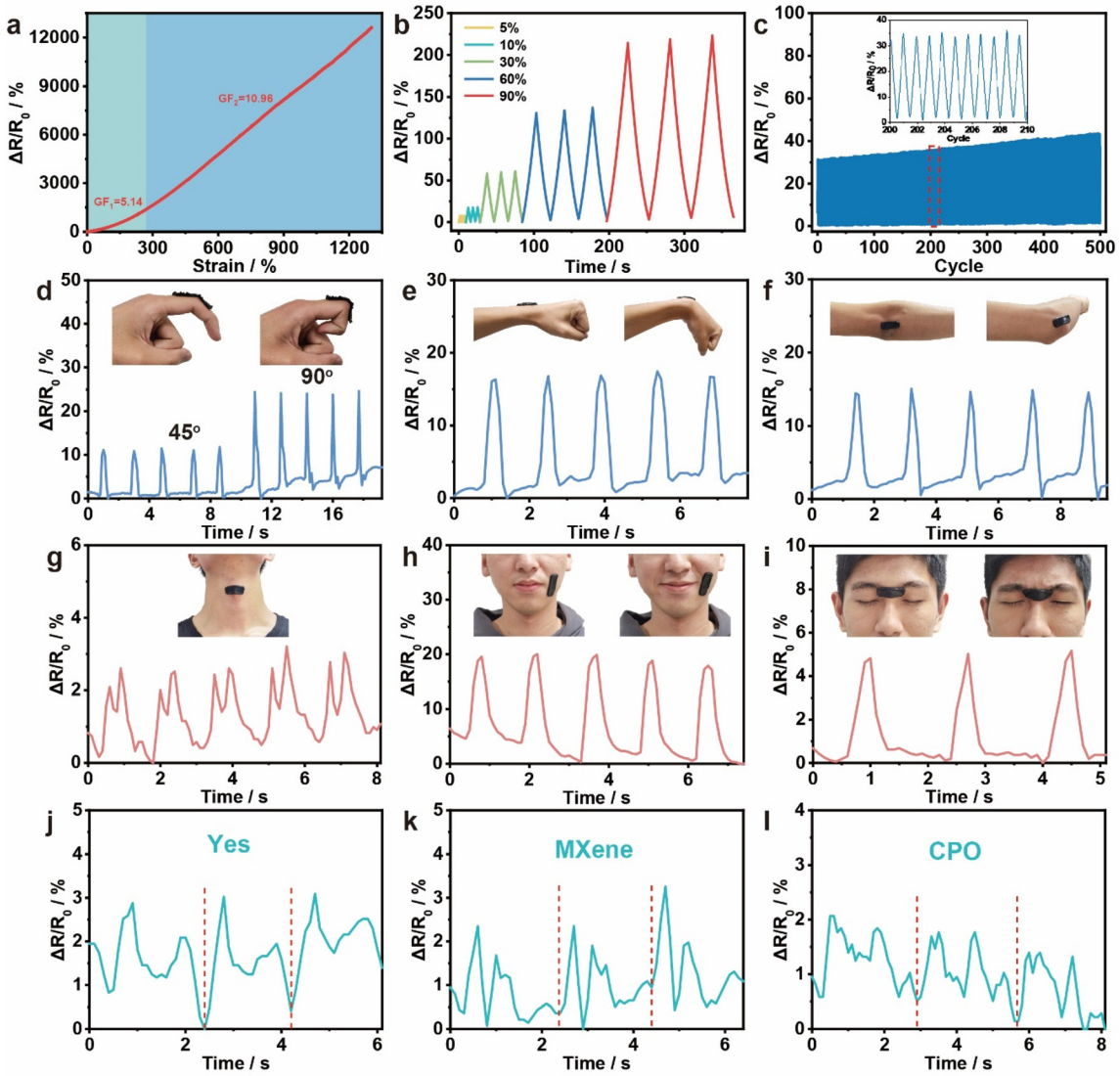

Fig. 4 Sensing performance of the MXene/PAA organohydrogel. (a) Relative resistance variation of the MXene/PAA organohydrogel at different strains. (b) Relative resistance variation under different strains (*i.e.*, 5%, 10%, 30%, 60% and 90%). (c) Relative resistance stability of the strain sensor for 500 s at a strain of 30%. Applications of MXene/PAA organohydrogel sensors. Real-time recording of the relative resistance changes generated by various human activities of the finger (d), wrist (e), elbow (f), throat (g), mouth (h), eyebrow (i) and throat pronunciation (j–l).

Application of the MXene/PAA organohydrogel strain sensor

A wireless HMI device is designed, utilizing the MXene/PAA organohydrogel as its primary sensing material. The internal circuit of the device is depicted in Fig. 5a. The device is comprised of the MXene/PAA organohydrogel, a wire, and a signal acquisition/transmission module (Fig. 5b). To use the device, the MXene/PAA organohydrogel is attached to the finger and the two ends of the hydrogel are connected to the signal acquisition/transmission module through electrode clips (Fig. 5c). The motion signal of the human finger is then displayed directly on a mobile phone screen (Fig. 5d). When the sensor was attached to the index finger to monitor finger flexion at different angles (45° and 90°), the relative resistance change was uniform. The relative resistance peak intensity changes were obvious, allowing for accurate tracking of changes in the

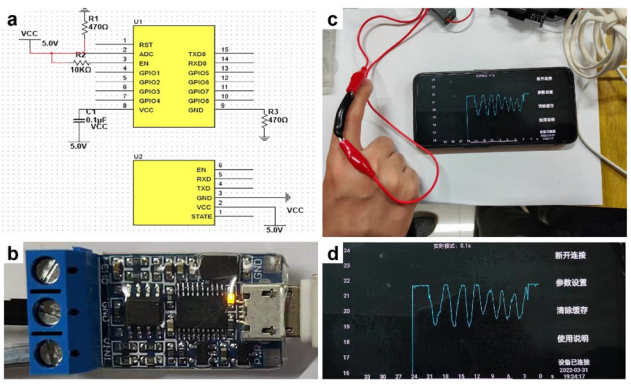

Fig. 5 The MXene/PAA organohydrogel sensor applied to wireless HMI sensor equipment, schematic diagram of the internal circuit (a), schematic diagram of the device connection (b), signal acquisition/transmission module (c), and mobile phone terminal signal display (d).

finger bending angle. These results demonstrate the feasibility and potential of the MXene/PAA organohydrogel-based sensor for use in wireless wearable HMI.

Conclusion

In conclusion, a multifunctional MXene/PAA organohydrogel that meets the challenging requirements of complex environments is successfully developed in this work. The organohydrogel has great puncture resistance, fast self-healing ability (~0.5 s), strong adhesiveness to different substrates, excellent frost resistance (−25 °C), and long-term moisturizing properties (>105 h). The corresponding flexible strain sensor demonstrates excellent sensing performance, including high sensitivity (GF ~10.96), wide detection range (0–1304%), and cycling stability (500 cycles). It can monitor different joint movements of the human body in real time with high reliability, and accurately capture physiological activities such as micro-expressions and throat pronunciation. The corresponding wireless HMI electronics demonstrate reliable practicality in real-time detection of human motion. This work promotes the field of wearable organohydrogel sensors and paves the way for the development of advanced practical sensing technologies.

Conflicts of interest

There are no conflicts to declare.

Acknowledgements

This work was supported by the National Natural Science Foundation of China (62174086, 62288102), and the Postgraduate Research & Practice Innovation Program of Jiangsu Province (KYCX23_0985).

References

1 L. Li, S. Zhao, W. Ran, Z. Li, Y. Yan, B. Zhong, Z. Lou, L. Wang and G. Shen, *Nat. Commun.*, 2022, **13**, 5975.
2 N. Kshetri and Y. K. Dwivedi, *Int. J. Inf. Manage.*, 2023, **69**, 102620.
3 J. Xu, X. Li, H. Chang, B. Zhao, X. Tan, Y. Yang, H. Tian, S. Zhang and T. L. Ren, *ACS Nano*, 2022, **16**, 6687–6699.
4 J. Yang, J. An, Y. Sun, J. Zhang, L. Zu, H. Li, T. Jiang, B. Chen and Z. L. Wang, *Nano Energy*, 2022, **97**, 107199.
5 S. Geng, S. Fan, H. Li, Y. Qi, C. An, E. Wu, J. Su and J. Liu, *Adv. Funct. Mater.*, 2023, 2302345.
6 T. Reid and J. Gibert, *Science*, 2022, **375**, 149–150.
7 W. Zhao, H. Ni, C. Ding, L. Liu, Q. Fu, F. Lin, F. Tian, P. Yang, S. Liu, W. He, X. Wang, W. Huang and Q. Zhao, *Nat. Commun.*, 2023, **14**, 278.
8 Z. Zhang, F. Wen, Z. Sun, X. Guo, T. He and C. Lee, *Adv. Intell. Syst.*, 2022, **4**, 2100228.
9 C. Wei, W. Lin, S. Liang, M. Chen, Y. Zheng, X. Liao and Z. Chen, *Nano-Micro Lett.*, 2022, **14**, 131.
10 F. Xu, X. Jin, C. Lan, Z. H. Guo, R. Zhou, H. Sun, Y. Shao, J. Meng, Y. Liu and X. Pu, *Nano Energy*, 2023, **109**, 108312.
11 A. Chae, G. Murali, S. Y. Lee, J. Gwak, S. J. Kim, Y. J. Jeong, H. Kang, S. Park, A. S. Lee, D. Y. Koh, I. In and S. J. Park, *Adv. Funct. Mater.*, 2023, **33**, 2213382.
12 Y. Long, Z. Wang, F. Xu, B. Jiang, J. Xiao, J. Yang, Z. L. Wang and W. Hu, *Small*, 2022, **18**, 2203956.
13 Y. Zhang, Z. Xu, Y. Yuan, C. Liu, M. Zhang, L. Zhang and P. Wan, *Adv. Funct. Mater.*, 2023, **33**, 2300299.
14 G. Tian, D. Yang, C. Liang, Y. Liu, J. Chen, Q. Zhao, S. Tang, J. Huang, P. Xu, Z. Liu and D. Qi, *Adv. Mater.*, 2023, **35**, 2212302.
15 H. Wang, X. Yi, T. Liu, J. Liu, Q. Wu, Y. Ding, Z. Liu and Q. Wang, *Adv. Mater.*, 2023, **35**, 2300394.
16 C. Xie, X. Wang, H. He, Y. Ding and X. Lu, *Adv. Funct. Mater.*, 2020, **30**, 1909954.
17 T. Qin, X. Li, A. Yang, M. Wu, L. Yu, H. Zeng and L. Han, *Chem. Eng. J.*, 2023, **461**, 141905.
18 B. Zhao, Z. Bai, H. Lv, Z. Yan, Y. Du, X. Guo, J. Zhang, L. Wu, J. Deng, D. W. Zhang and R. Che, *Nano-Micro Lett.*, 2023, **15**, 79.
19 J.-Y. Yu, S. E. Moon, J. H. Kim and S. M. Kang, *Nano-Micro Lett.*, 2023, **15**, 51.
20 H. Fu, B. Wang, J. Li, J. Xu, J. Li, J. Zeng, W. Gao and K. Chen, *Mater. Horiz.*, 2022, **9**, 1412–1421.
21 H. Ding, Z. Wu, H. Wang, Z. Zhou, Y. Wei, K. Tao, X. Xie and J. Wu, *Mater. Horiz.*, 2022, **9**, 1935–1946.
22 H. Wang, X. Li, Y. Ji, J. Xu, Z. Ye, S. Wang and X. Du, *J. Mater. Chem. B*, 2022, **10**, 2933–2943.
23 Y. Zhao, N. Yang, X. Chu, F. Sun, M. U. Ali, Y. Zhang, B. Yang, Y. Cai, M. Liu, N. Gasparini, J. Zheng, C. Zhang, C. Guo and H. Meng, *Adv. Mater.*, 2023, **35**, 2211617.
24 Y. Liu, Q. Liu, L. Zhong, C. Chen and Z. Xu, *Chem. Eng. J.*, 2023, **452**, 139314.
25 X.-Q. Wang, K. H. Chan, W. Lu, T. Ding, S. W. L. Ng, Y. Cheng, T. Li, M. Hong, B. C. K. Tee and G. W. Ho, *Nat. Commun.*, 2022, **13**, 3369.
26 J. Wang, F. Tang, C. Yao and L. Li, *Adv. Funct. Mater.*, 2023, **33**, 2214935.
27 J. Wu, W. Huang, Z. Wu, X. Yang, A. G. P. Kottapalli, X. Xie, Y. Zhou and K. Tao, *ACS Mater. Lett.*, 2022, **4**, 1616–1629.
28 C. Cai, C. Wen, W. Zhao, S. Tian, Y. Long, X. Zhang, X. Sui, L. Zhang and J. Yang, *ACS Appl. Mater. Interfaces*, 2022, **14**, 23692–23700.
29 Y. Wu, J. Qu, X. Zhang, K. Ao, Z. Zhou, Z. Zheng, Y. Mu, X. Wu, Y. Luo and S. P. Feng, *ACS Nano*, 2021, **15**, 13427–13435.
30 Y. Yu, P. Yi, W. Xu, X. Sun, G. Deng, X. Liu, J. Shui and R. Yu, *Nano-Micro Lett.*, 2022, **14**, 77.
31 H. Liao, X. Guo, P. Wan and G. Yu, *Adv. Funct. Mater.*, 2019, **29**, 1904507.

32 Y. Wei, L. Xiang, H. Ou, F. Li, Y. Zhang, Y. Qian, L. Hao, J. Diao, M. Zhang, P. Zhu, Y. Liu, Y. Kuang and G. Chen, *Adv. Funct. Mater.*, 2020, **30**, 2005135.
33 G. Wang, Q. Zhang, Q. Wang, L. Zhou and G. Gao, *ACS Appl. Mater. Interfaces*, 2021, **13**, 24173–24182.
34 W. Zhao, J. Peng, W. Wang, B. Jin, T. Chen, S. Liu, Q. Zhao and W. Huang, *Small*, 2019, **15**, 1901351.
35 H. Lin, S. Ma, B. Yu, X. Pei, M. Cai, Z. Zheng, F. Zhou and W. Liu, *Chem. Mater.*, 2019, **31**, 9504–9512.
36 Q. Wang, X. Pan, C. Lin, H. Gao, S. Cao, Y. Ni and X. Ma, *Chem. Eng. J.*, 2020, **401**, 126129.
37 Y. Jiao, Y. Lu, K. Lu, Y. Yue, X. Xu, H. Xiao, J. Li and J. Han, *J. Colloid Interface Sci.*, 2021, **597**, 171–181.
38 H. Sun, Y. Zhao, S. Jiao, C. Wang, Y. Jia, K. Dai, G. Zheng, C. Liu, P. Wan and C. Shen, *Adv. Funct. Mater.*, 2021, **31**, 2101696.
39 Z. Zhang, D. Li, W. Jiang and Z. Wang, *Adv. Phys.: X*, 2018, **3**, 1428915.
40 X. Li, L. He, Y. Li, M. Chao, M. Li, P. Wan and L. Zhang, *ACS Nano*, 2021, **15**, 7765–7773.
41 H. Wang, X. Yu, X. Tang, Y. Sun, X. Zeng and L. Lin, *Cellulose*, 2022, **29**, 341–354.
42 Y. Bai, S. Bi, W. Wang, N. Ding, Y. Lu, M. Jiang, C. Ding, W. Zhao, N. Liu, J. Bian, S. Liu and Q. Zhao, *Soft Mater.*, 2022, **20**, 444–454.
43 J. Yang, Z. Liu, K. Li, J. Hao, Y. Guo, M. Guo, Z. Li, S. Liu, H. Yin, X. Shi, G. Qin, G. Sun, L. Zhu and Q. Chen, *ACS Appl. Mater. Interfaces*, 2022, **14**, 39299–39310.
44 P. Xue, C. Valenzuela, S. Ma, X. Zhang, J. Ma, Y. Chen, X. Xu and L. Wang, *Adv. Funct. Mater.*, 2023, **33**, 2214867.
45 Y. Bai, Y. Lu, S. Bi, W. Wang, F. Lin, F. Zhu, P. Yang, N. Ding, S. Liu, W. Zhao, N. Liu and Q. Zhao, *Adv. Mater. Technol.*, 2023, **8**, 2201767.